# CHAPTER-5

## Replacing anodic oxygen evolution reaction with benzyl alcohol oxidation using Prussian blue analogues


**5.1. Abstract**

The overall water splitting suffers from high energy input, low efficiency, sluggish OER kinetics, and the mixing of $H_2$ and $O_2$, leading to potential safety hazards. Therefore, the replacement of anodic OER with a thermodynamically more favorable organic oxidation reaction could be an important strategy to improve energy efficiency and lower the required overpotential. Herein, we have demonstrated the replacement of the anodic OER with electrocatalytic benzyl alcohol (BA) oxidation. First, electrochemical activation of the precatalysts CoCo-PBA@NF (PC-6) and CoFe-PBA@NF (PC-7) has been carried out to form corresponding active catalysts $Co(OH)_2$-Co(O)OH (AC-11) and Fe-$Co(OH)_2$-Co(O)OH (AC-12), respectively. The AC-12 delivered industrial scale current density (400 mA $cm^{-2}$) at only 1.47 V potential without interference from OER. The AC-12 showed a aradaic efficiency of 98.3% with a 0.34 mmol $h^{-1}$ conversion rate of BA.

## 5.2. Introduction

In recent years, overall water splitting has become an important strategy for the production of $H_2$ and $O_2$ [11,275]. However, the overall water splitting experiences the requirement of a huge amount of potential, poor energy efficiency, sluggish reaction kinetics of anodic OER, low current density, and mixing of $H_2$ and $O_2$ [276–278]. In this respect, the anodic OER could be replaced with electrocatalytic organic oxidation reactions to solve the above-mentioned issues. In addition, the electrochemical HER activity can be cost-effective when integrated with electrocatalytic organic oxidation reactions instead of OER [276–280]. Electrocatalytic organic oxidation not only improves the energy efficiency and the required potential but also produces high-value-added oxidized products at the anode [276–278].

In this respect, the replacement of anodic OER with BA oxidation has been explored in several studies resulting in the formation of value-added product benzoic acid as well as $H_2$ [276–280]. The anodic oxidation of BA is accomplished with the input of 0.48 V *vs* RHE in contrast to the 1.23 V *vs* RHE of OER [281–283]. Further, the integration of BA oxidation with HER results in a huge improvement in the $H_2$ evolution efficiency [276–280]. The replacement of the high-cost traditional synthesis process of benzoic acid in chemical, pharmaceutical, cosmetic as well as polymer industries requires the development of the green route of electrocatalytic oxidation [276–283].

In the past few years, the electrocatalytic oxidation of BA has led to the investigation of a series of electrocatalysts based on transition metals as well as noble metals [281-283]. In most of the studies, the BA oxidation has been operated at a low current density (<200 mA $cm^{-2}$) to avoid interference from OER [281–283]. The operation at a high current density leads to the production of $O_2$ at the anode, which further reduces the energy efficiency as well as the formation of value-added products [281–283]. Moreover,

the high current density for anodic organic oxidation at a high potential also diminishes the faradaic efficiency. Therefore, the designing of efficient electrocatalysts is crucial to achieve the industrial level current density (>400 mA $cm^{-2}$) for BA oxidation without the interference of OER [281–283].

Recently, M(O)OH active catalysts have been demonstrated for the anodic BA oxidation integrated with electrochemical $H_2$ evolution [276,278,280,283,284]. For example, NiCo-(oxy)hydroxide was prepared for the anodic BA oxidation producing industrial scale current density [283]. The excellent FE efficiency as well as the conversion of BA into benzoic acid was realized with NiCo-(oxy)hydroxide without interference from OER. Further, Au/CoOOH was also synthesized for the industrial scale BA oxidation [284]. The Au/CoOOH showed an improvement in the $H_2$ evolution efficiency by the replacement of anodic OER with BA oxidation.

As we have demonstrated a series of self-supported Fe-$Co(OH)_2$-Co(O)OH active catalysts by the anodic reconstruction of PBAs for efficient electrochemical water splitting, we have attempted to explore the electrocatalytic BA oxidation with self-supported PBA-derived Fe-$Co(OH)_2$-Co(O)OH catalysts (Figure 5.1a). The self-supported CoCo-PBA (PC-6) and CoFe-PBA (PC-7) were developed and further reconstructed under the applied anodic potential in CV conditions to form the active catalysts AC-11 and AC-12, respectively (Figure 5.1b).

The following objectives have been addressed in this chapter:

(i) We have employed the electrochemically reconstructed self-supported PBA-derived AC-11 and AC-12 catalysts for anodic BA oxidation by replacing kinetically sluggish OER (Figure 5.1c). The reconstructed active catalysts have been utilized for the electrocatalytic BA oxidation at the anode-producing industrial level current density (>400 mA $cm^{-2}$) without the interference of OER.

(ii) The effect of doping of Fe in the active catalyst on the catalytic activity and conversion of the BA has been studied. Further, the superior performance of PBA-derived electrochemically reconstructed active catalysts over the CoFe-LDH@NF, prepared by the hydrothermal method has been evaluated for the electrochemical BA oxidation.

(iii) The optimum potential and time for the full conversion of BA into benzoic acid have been examined using the AC-12 catalyst. Further, the improvement in $H_2$ evolution efficiency has also been established when the anodic OER was replaced with thermodynamically favorable BA oxidation.

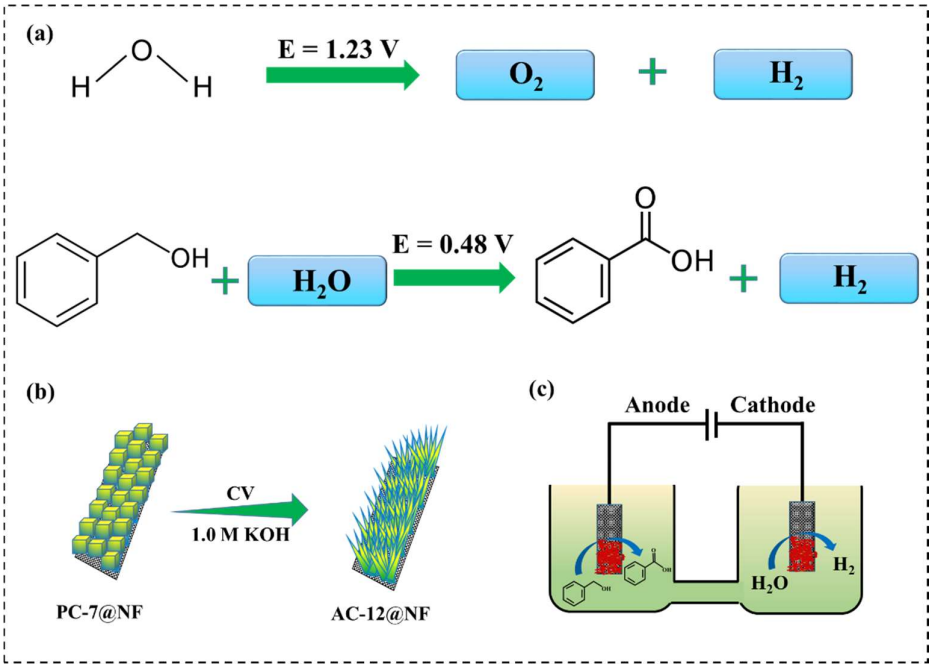


**Figure 5.1.** (a) Schematic depiction for the electrocatalytic benzyl alcohol oxidation by replacing the OER; (b) electrochemical reconstruction of PC-7 into AC-12 using cyclic voltammetry in 1.0 M KOH solution; and (c) integration of cathodic hydrogen evolution reaction with BA oxidation reaction at the anode by replacing OER.

### 5.3. Chemicals

The nickel foam (NF) was purchased from AXYS Technology Pvt. Ltd. West Bengal,

India. The chemicals used were already mentioned in chapter 2 (section 2.3).

### 5.4. Instruments

The instruments utilized for the characterization of the synthesized catalysts were described in chapter 2 (section 2.4).

### 5.5. Experimental

#### 5.5.1. Synthesis of cobalt hydroxide on nickel foam (CoHC@NF)

The nickel foam was cut into pieces of size 1 cm × 2 cm and washed with acetone and water. Further, the pieces of nickel foams were ultra-sonicated with 3.0 M HCl for 15 min to remove the surface impurities. The CoHC@NF films were prepared by adopting the same procedure as employed for the synthesis of CoHC@CC in chapter 2 (section 2.5). The NF was used in place of CC for the synthesis of CoHC@NF.

#### 5.5.2. Synthesis of precatalyst PC-6 and PC-7

For the synthesis of PC-7, $K_3[Fe(CN)_6]$ (0.4 mmol) was mixed into 5 mL of $H_2O$ in a glass vial. The CoHC@NF film was put vertically inside the vial and left for 1 h at RT. After 1 h, the vial was capped and heated at 60 $^oC$ for 6 h. After the natural cool down, the CoFe-PBA@NF film (denoted as PC-7) was collected from the vial and washed with $H_2O$ three times followed by drying at 50 $^oC$ for 12 h. Similarly, the PC-6 was synthesized by replacing $K_3[Fe(CN)_6]$ with $K_3[Co(CN)_6]$.

#### 5.5.3. Synthesis of CoFe-LDH on nickel foam (CoFe-LDH@NF)

The CoFe-LDH@NF was prepared by using a procedure similar to the synthesis of CoFe-LDH@CC as mentioned in chapter 2 (section 2.5). The CC was replaced by the NF to synthesize CoFe-LDH@NF.

#### 5.5.4. Electrochemical measurements

The electrochemical measurement details were explained in chapter 2 (section 2.6).

**Table 5.1.** Details of electrochemically reconstructed active catalysts synthesized by CV treatment of PC-6 and PC-7.

| Precatalyst | Active catalyst | Denoted name | Reaction conditions |
|---|---|---|---|
| PC-6 | $Co(OH)_2$-Co(O)OH | AC-11 | CV, 1-2 V *vs* RHE |
| PC-7 | Fe-$Co(OH)_2$-Co(O)OH | AC-12 | CV, 1-2 V *vs* RHE |

### 5.6. Conditions for benzyl alcohol oxidation

It is crucial to operate the BA oxidation at a lower potential than the onset of OER to avoid its interference. As AC-12 showed OER onset at 1.52 V vs RHE potential, we have performed electrochemical oxidation of BA in a three-electrode system at a constant potential of 1.50 V *vs* RHE for 3 h under chronoamperometric conditions. The OER onset potential and BA oxidation potential of the active catalysts have been summarized in Table 5.2. The active catalysts were utilized as working electrodes while Pt wire and Ag/AgCl were employed as counter and reference electrodes, respectively. The BA oxidation was carried out using 10 mL of 0.1 M BA in a customized electrochemical cell. Further, the potential (1.48 V and 1.45 V) for the BA oxidation was also varied to investigate the effect on the conversion of BA. Due to the excellent conversion efficiency at 1.50 V, the BA oxidation was also carried out using AC-11 and hydrothermally prepared CoFe-LDH@NF for 3 h to examine the conversion efficiency. The toluene was utilized for the extraction of the products, which were analyzed by $^1$H NMR spectroscopy.

**Table 5.2.** Details of onset potential and BA oxidation potential of the electrochemically reconstructed active catalysts.

| Active catalyst | OER Onset | BA oxidation potential |
|---|---|---|
| AC-11 | 1.52 V *vs* RHE | 1.50 V *vs* RHE |
| AC-12 | 1.52 V *vs* RHE | 1.50 V *vs* RHE |

### 5.7. Separation of benzoic acid

The conversion of benzoic acid into potassium benzoate was detected in the presence of KOH after the reaction. Therefore, 3.0 M HCl was poured into the electrolyte for the formation of benzoic acid from potassium benzoate. The benzoic acid crystals were filtered and dried at 60 $^{o}$C for 30 minutes. As the benzoic acid had the impurity of KCl, a recrystallization process was used for the removal of KCl. The crystals of benzoic acid were dissolved in the hot water (80 $^{o}$C) and cooled down slowly. After natural cooling, the recrystallized crystals of pure benzoic acid were filtered and dried at 60 $^{o}$C.

### 5.8. Determination of faradaic efficiency for benzyl alcohol oxidation

We have calculated the faradaic efficiency by using the weight of the BA utilized for the oxidation and the charge passed throughout the reaction. As we have determined the full conversion of BA into benzoic acid within 3 h, the required charge for full conversion ($Q_{100\%\ FE}$) can be calculated by:

$$Q_{100\%\ FE} = \frac{m_{BA} \times F \times n_e}{M_{BA}}$$

Where F represents Faraday constant (96485 C mol$^{-1}$), $n_e$ indicates the number of electrons transferred involved in the oxidation (4), $m_{BA}$ is the weight of BA used for the oxidation (112.32 mg) and $m_{BA}$ denotes the molecular weight of BA (108.14 g mol$^{-1}$). From the calculations, we have obtained $Q_{100\%\ FE}$ = 400.85 C. As the purity of BA is 99% (taken from Alfa Aesar), the $Q_{100\%\ FE}$ can be determined to be 396.84 C. The charge passed for the 100% oxidation of BA after 3 h was determined to be 393.54 C. Therefore, the faradaic efficiency of 99.1% was calculated by taking the quotient of these charges.

### 5.9. Results and discussion

#### 5.9.1. Characterizations of precatalysts PC-6 and PC-7

The precatalysts were characterized using spectroscopic and microscopic techniques and the formation of PBA precatalysts was well established with PXRD, IR, SEM, TEM, and

EDX studies. The FTIR spectra of PC-6 and PC-7 detected the peaks at 2170-2130 $cm^{-1}$ for the bridging –CN groups in PBAs (Figure 5.2a) [285–287]. The PXRD patterns evidenced that the PC-6 and PC-7 had the cubic crystal structure (JCPDF No-01-077-1161) (Figure 5.2b). SEM and TEM images analyzed the cubic morphology of both the PC-6 and PC-7 (Figure 5.2c-f). EDX spectra identified the Co, Fe, C, N, and O elements in PC-7 and Co, N, C, and O elements in PC-6 (Figure 5.2g-h).

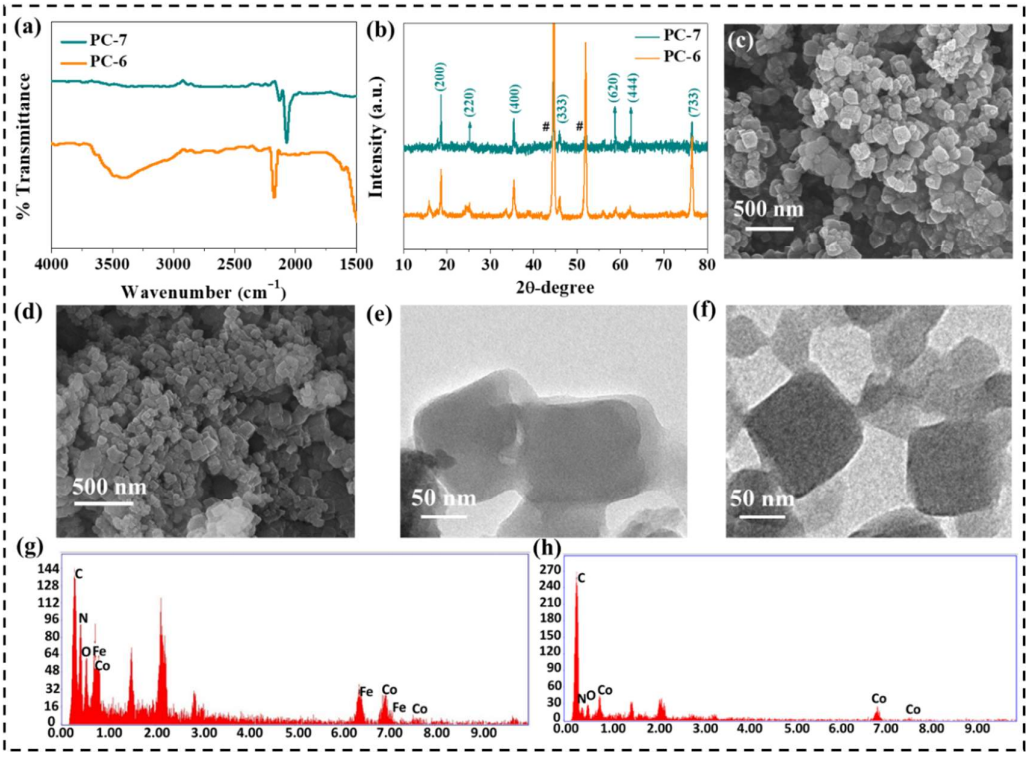


**Figure 5.2.** (a) IR spectra of PC-6 and PC-7; (b) PXRD pattern of PC-6 and PC-7; (c) SEM image of PC-7; (d) SEM image of PC-6; (e) TEM image of PC-7; (f) TEM image of PC-6; (g) EDX spectra of PC-7 and (h) EDX spectra of PC-6.

### 5.9.2. Electrochemical reconstruction of precatalyst PC-6 and PC-7

The bulk reconstruction of PC-6 and PC-7 was performed similar to the PC-2 as mentioned in chapter-2 (section 2.3). The CV reconstruction was carried out for 200

cycles where the PC-6 and PC-7 were reconstructed electrochemically to produce AC-11 and AC-12 active catalysts, respectively. Similar to the CV reconstruction of PC-2 and PC-3, the electrochemical CV reconstruction was carried out in 1.0 M KOH solution at the scan rate of 20 mV $s^{-1}$.

### 5.9.3. Characterizations of active catalysts AC-11 and AC-12

The spectroscopy and microscopy established that the electrochemical reconstruction of PC-6 and PC-7 led to the $Co(OH)_2$-Co(O)OH (AC-11) and Fe-$Co(OH)_2$-Co(O)OH (AC-12) catalysts with ultrathin nanosheet morphology. Firstly, IR spectra realized the absence of the peaks for the bridged -CN groups after CV reconstruction (Figure 5.3a) [82,178]. The PXRD pattern of AC-11 and AC-12 evidenced the peaks, which were matched with the mixed phase of α-$Co(OH)_2$ (JCPDF No-48-0083) and β-Co(O)OH (JCPDF No-26-0480) (Figure 5.3b).

The Co 2p XPS of AC-11 unveiled the peaks for Co $2p_{3/2}$ and Co $2p_{1/2}$ at 780.21 eV and 795.81 eV, respectively (Figure 5.3c) [287–289]. The two peaks fitted at 780.31 eV and 781.38 eV were identified for $Co^{3+}$ and $Co^{2+}$ in AC-11, respectively. The Co $2p_{3/2}$ peak of AC-12 was shifted by 0.59 eV towards higher binding energy in contrast to the AC-11. The higher $Co^{3+}/Co^{2+}$ ratio of 3.12 was calculated for AC-12 while AC-11 possessed $Co^{3+}/Co^{2+}$ ratio of 2.89 [64,65]. Further, spin-orbit coupling spacing indicated the value of 15.20 eV suggesting the high amount of $Co^{3+}$ in AC-12 compared to the AC-11 (15.50 eV) [287–289].

The Fe 2p XPS of AC-12 detected the peaks for Fe $2p_{3/2}$ and Fe $2p_{1/2}$ at 708.7 eV and 721.6 eV, respectively (Figure 5.3d) [65,82]. The peaks at 710.81 eV and 711.45 eV confirmed the existence of $Fe^{2+}$ and $Fe^{3+}$ species in AC-12. The O 1s XPS of AC-11 also revealed the prominent peaks for the M-O bond, surface –OH groups, and adsorbed water molecules at 529.21 eV, 531.57 eV, and 532.32 eV, respectively (Figure 5.3e)

[82,86,287,289]. The O 1s XPS of AC-12 identified the characteristic peaks at 531.43 eV and 532.51 eV corresponding to the absorbed $H_2O$ as well as surface –OH groups, respectively (Figure 5.3f). Additionally, the peak for the metal-oxygen bond was appeared at 529.37 eV in AC-12.

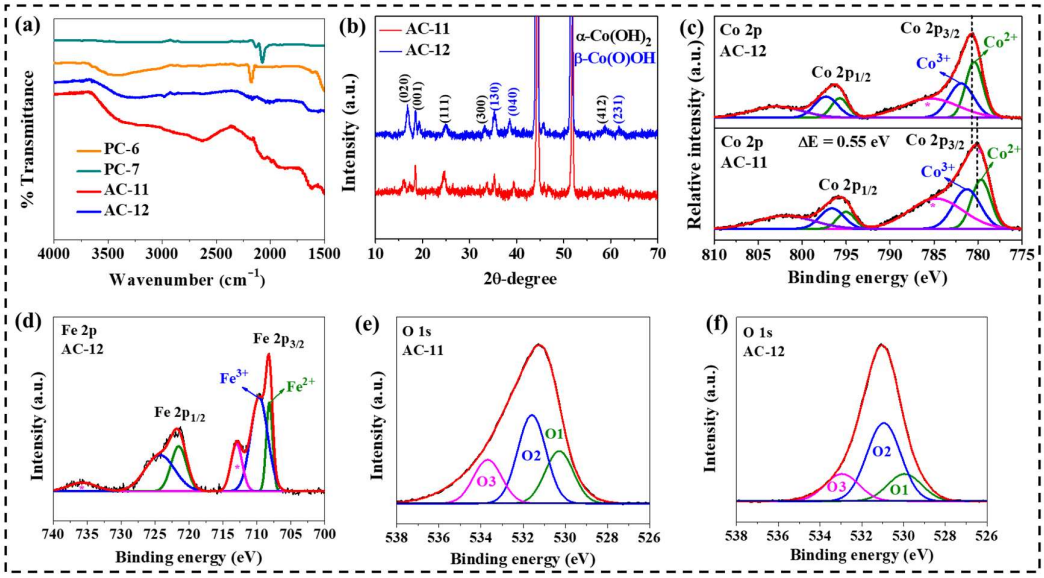


**Figure 5.3.** (a) IR spectra of AC-11 and AC-12 compared with PC-6 and PC-7; (b) PXRD pattern of AC-11 and AC-12; (c) comparison of Co 2p XPS of AC-11 and AC-12; (d) Fe 2p XPS of AC-12; (e) O 1s XPS of AC-11 and (f) O 1s XPS of AC-12.

TEM images revealed the ultrathin transparent nanosheets of AC-11 and AC-12 (Figure 5.4a-b). HRTEM image of AC-12 presented the well-resolved lattice spacing with a d-value of 0.23 nm for the (111) plane in β-Co(O)OH (JCPDF No-26-0480) (Figure 5.4c). In the case of HRTEM of AC-11, the d-spacing value of 0.23 nm was also determined for the (111) plane of β-Co(O)OH (JCPDF No-26-0480) (Figure 5.4d).

### 5.9.4. Electrochemical performance

The electrochemical performance of the AC-11 and AC-12 was assessed in 1.0 M aqueous KOH solution with 0.1 M BA. The LSV profile revealed the improvement in the

current density and overpotential for the BA oxidation compared to the OER for both active catalysts. The AC-12 afforded an industrial level current density of 400 mA $cm^{-2}$ for BA oxidation at only 1.47 V potential compared to the OER (Figure 5.5a). In contrast, AC-11 delivered the same current density for BA oxidation at a 1.56 V potential higher than AC-12 but lower than that of OER. The poor catalytic performance of hydrothermally prepared CoFe-LDH@NF was also analyzed for BA oxidation compared to the PBA-derived AC-12.

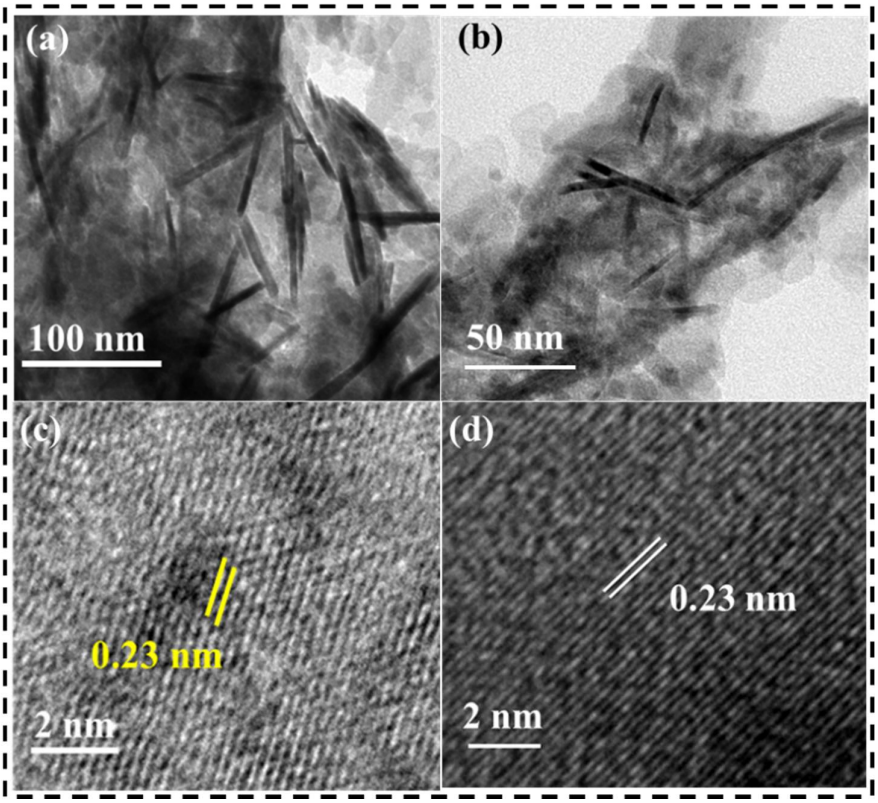


**Figure 5.4.** (a) TEM image of AC-12; (b) TEM image of AC-11; (c) HRTEM image of AC-12 and (d) HRTEM image of AC-11.

The catalyst should be operated for BA oxidation at a lower potential than the onset of OER to afford the industrial level current density (400 mA $cm^{-2}$) avoiding interference from OER. This enhances the overall FE for BA oxidation. In this work, our PBA-derived

AC-12 demonstrated the industrial level current density of 400 mA $cm^{-2}$ at only 1.47 V potential without the occurrence of OER. Moreover, BA oxidation was performed at a 1.50 V potential lower than the OER onset potential. Notably, AC-12 attained 1 A $cm^{-2}$ current density at 1.49 V for BA oxidation without the interference of OER (Figure 5.5a). The AC-12 realized the outstanding BA oxidation activity compared to the literature-reported catalysts.

To evaluate the superiority of electrochemically reconstructed active catalyst, the catalytic activity of AC-12 was also compared with hydrothermally prepared CoFe-LDH@NF. The LSV profile for the BA oxidation demonstrated the best activity of electrochemically reconstructed AC-12 over the hydrothermally prepared CoFe-LDH@NF (Figure 5.5b). The EIS plot unveiled the lower $R_{ct}$ value for AC-12 (1.0 Ω) in contrast to the AC-11 (1.2 Ω) (Figure 5.5c). The larger $C_{dl}$ value of 2.93 mF $cm^{-2}$ was also calculated for AC-12 while the $C_{dl}$ value of 2.24 mF $cm^{-2}$ was determined for AC-11 (Figure 5.5d). Larger $C_{dl}$ value revealed the larger number of active sites in AC-12, which led to the facile adsorption properties on the surface.

Further, improvement in the hydrogen evolution efficiency was examined when the anodic OER was replaced with the BA oxidation. The amount of $H_2$ produced at 1.50 V with or without BA was determined by the water displacement method using an H-type cell. Interestingly, the plot evidenced that the evolution of $H_2$ was increased by three times when the anodic OER was replaced with BA oxidation (Figure 5.5e). This result verified that the coupling of HER with BA oxidation improved the $H_2$ evolution efficiency. The CA measurement was carried out at a fixed potential of 1.50 V *vs* RHE up to 3 h for BA oxidation using AC-12 catalyst. The plot for the conversion of BA into benzoic acid indicated that the 100% formation of benzoic acid was demonstrated within 3 h (Figure 5.5f).

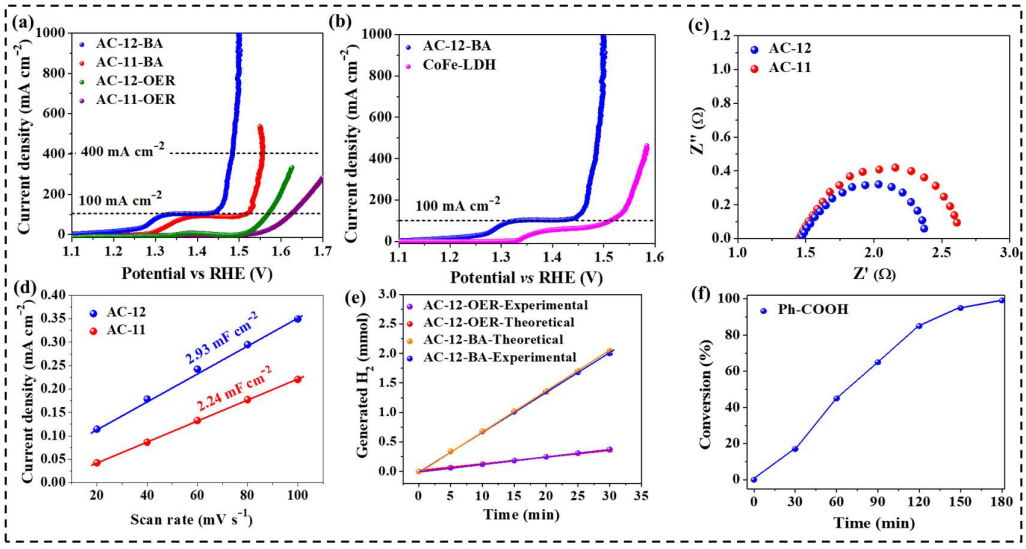


**Figure 5.5.** (a) LSV profiles for the OER activity and BA oxidation activity of AC-11 and AC-12; (b) LSV profiles for the BA oxidation activity of AC-12 and CoFe-LDH@NF; (c) EIS plot of AC-11 and AC-12; (d) $C_{dl}$ plot of AC-11 and AC-12; (e) FE measurement at 1.50 V *vs* RHE with or without BA showing the improvement in the hydrogen evolution efficiency and (f) plot for the time-dependent formation of benzoic acid.

As the BA oxidation with AC-12 was performed at 1.50 V for 3 h, the LSV was recorded after 3 h at the completion of the reaction. Interestingly, the LSV curve after 3 h of BA oxidation was almost identical to the LSV curve of OER (Figure 5.6a).

This result further clarified that the BA was absent in the electrolyte after 3 h of the reaction and the OER was started further in the absence of BA. The excellent stability of the AC-12 was determined by repeating the BA oxidation under CA at 1.50 V potential. The LSV plot after each cycle of CA revealed that the overpotential and current density remained constant for the five successive cycles (Figure 5.6b). This indicated the excellent stability of AC-12 for BA oxidation. The excellent FE for the formation of benzoic acid was also recorded for each cycle (Figure 5.6c).

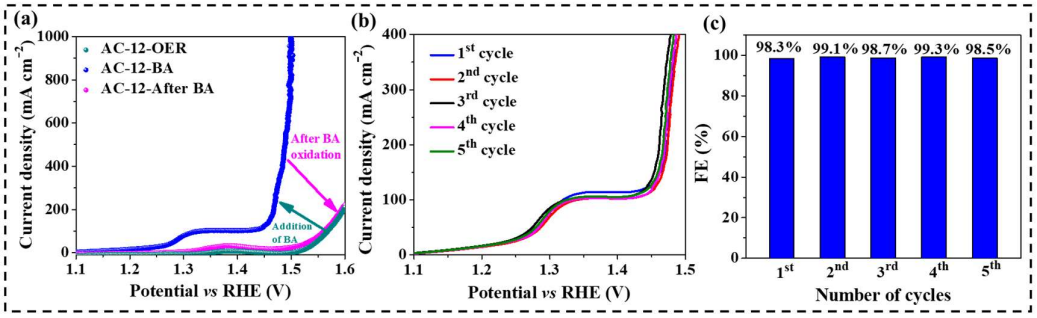


**Figure 5.6.** (a) LSV profiles for the OER activity and BA oxidation activity of AC-12 compared with LSV after BA oxidation; (b) LSV profiles for the BA oxidation activity using AC-12 for five successive cycles and (c) FE plot for the BA oxidation using AC-12 for five successive cycles.

### 5.9.5. Analysis of BA oxidation

The $^{1}$H NMR spectra were utilized to detect the conversion of reactant as well as formed products after 3 h (Figure 5.7a). The peak at ~11.67 ppm was observed for the acidic proton of benzoic acid. Any other byproduct or reactant was not detected after 3 h indicating the 100% selectivity of BA oxidation to benzoic acid. The potential (1.48 V and 1.45 V) for the BA oxidation was also varied to investigate the effect on the conversion of BA. Interestingly, 95% and 89% conervsion of BA was achieved at 1.48 V and 1.45 V, respectively, with AC-12. Further, BA oxidation with AC-11 was also performed at 1.50 V potential and 82% conversion of BA into benzoic acid was achieved after 3 h. Further, CoFe-LDH@NF indicated the 75% conversion of BA into benzoic acid under similar conditions.

## 5.10. Conclusions

In summary, we have successfully employed the self-supported PBA-derived AC-11 and AC-12 catalysts for electrocatalytic BA oxidation reaction at the anode. The electrochemically reconstructed AC-12 afforded an industrial level current density of 400

mA $cm^{-2}$ at only 1.47 V potential for BA oxidation. The active catalyst AC-12 outperfomed AC-11 and hydrothermally prepared CoFe-LDH for BA oxidation. The catalyst AC-12 showed ~100% conversion of 0.1 M BA into benzoic acid at 1.50 V potential within 3 h. Moreover, AC-12 attained excellent FE of 98.3% while the rate of BA oxidation was determined to be 0.34 mmol $h^{-1}$.

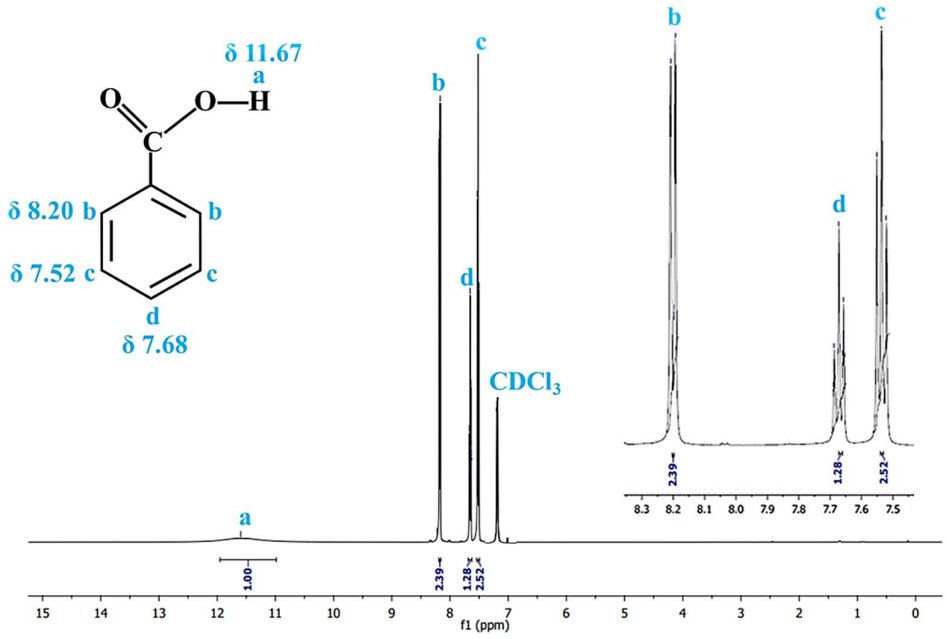


**Figure 5.7.** $^{1}H$ NMR spectra of the product after 3 h of BA oxidation using AC-12.